Repulsive inter-layer coupling induces anti-phase synchronization

Cite as: Chaos **31**, 063116 (2021); doi: 10.1063/5.0054770
Submitted: 21 April 2021 · Accepted: 25 May 2021 ·
Published Online: 14 June 2021

Igor A. Shepelev,[1,a)] Sishu S. Muni,[2,b)] Eckehard Schöll,[3,c)] and Galina I. Strelkova[1,d)]

AFFILIATIONS

[1]Institute of Physics, Saratov State University, 83 Astrakhanskaya Street, Saratov 410012, Russia
[2]School of Fundamental Sciences, Massey University, Palmerston North 4410, New Zealand
[3]Institut für Theoretische Physik, Technische Universität Berlin, Hardenbergstr. 36, 10623 Berlin, Germany

Note: This paper is part of the Focus Issue, In Memory of Vadim S. Anishchenko: Statistical Physics and Nonlinear Dynamics of Complex Systems.

[a)]**Author to whom correspondence should be addressed:** igor_sar@li.ru
[b)]**Electronic mail:** s.muni@massey.ac.nz
[c)]**Electronic mail:** schoell@physik.tu-berlin.de
[d)]**Electronic mail:** strelkovagi@sgu.ru

ABSTRACT

We present numerical results for the synchronization phenomena in a bilayer network of repulsively coupled 2D lattices of van der Pol oscillators. We consider the cases when the network layers have either different or the same types of intra-layer coupling topology. When the layers are uncoupled, the lattice of van der Pol oscillators with a repulsive interaction typically demonstrates a labyrinth-like pattern, while the lattice with attractively coupled van der Pol oscillators shows a regular spiral wave structure. We reveal for the first time that repulsive inter-layer coupling leads to anti-phase synchronization of spatiotemporal structures for all considered combinations of intra-layer coupling. As a synchronization measure, we use the correlation coefficient between the symmetrical pairs of network nodes, which is always close to −1 in the case of anti-phase synchronization. We also study how the form of synchronous structures depends on the intra-layer coupling strengths when the repulsive inter-layer coupling is varied.

Synchronous behavior in large and complex ensembles of oscillators is considered to be one of the basic mechanisms in stable and proper functioning of real-world systems in many areas, ranging from technology and engineering to biology, neuroscience, and socio-economic systems.[1–8] Recently, in the framework of the concept of multilayer networks,[9,10] various scenarios of synchronization have been intensively studied.[11–29] Since real-world systems usually interact in different ways, special attention has been paid to the impact of various types of the coupling topology on the network dynamics and synchronization phenomena.[14,23–27,30–34] Most of this research has focused on attractively coupled networks, and only little literature covers the issue of repulsive coupling[35–41] or mixed networks,[42–46] which represent a combination of attractive and repulsive elements. Moreover, a purely repulsive interaction between layers in multiplex networks has not been explored at all. Here, we investigate synchronization of a multiplex two-layer network of 2D lattices of locally coupled van der Pol oscillators with a repulsive interaction between the layers. We show for the first time that the repulsive inter-layer coupling induces anti-phase synchronization of spatiotemporal structures in the network under study. This is independent of the type of intra-layer coupling, which may be attractive, favoring spiral waves, or repulsive, favoring labyrinth-like patterns.[47] Synchronous regimes are quantified using the correlation coefficient between the corresponding pairs of the network nodes. This measure is always close to −1 for anti-phase synchronization. We also study how the synchronous structures change when the intra-layer and inter-layer coupling strengths are varied.

I. INTRODUCTION

Synchronization phenomena in interacting dynamical systems and networks are of great relevance with respect to both

the fundamental knowledge in synergetics[1–6] and their broad applications in technology and engineering,[7,48,49] neuroscience,[50–53] sociology,[54] economics,[55] epidemiology,[56,57] etc. Synchronization is essential to keep vital systems and processes staying stable and running smoothly, but sometimes it is also undesirable. A great deal of research studies have been done to uncover the mechanisms of synchronization with the aim to find the best way to achieve and improve synchronization in complex systems and networks.[58–60]

Recently, much attention of the researchers has been paid to studying synchronization, which results from the interaction between networks with complex topology.[6] Thus, the concept of multilayer networks[9,10,61,62] becomes widely used since real-world systems are, as a rule, multi-components and characterized by different coupling topologies both within layers and between them.

In the context of multilayer networks, different forms of synchronization have been revealed and explored, such as cluster synchronization,[11,12] inter-layer and intra-layer synchronization,[13–16] explosive synchronization,[17–20] generalized synchronization,[63] forced and mutual synchronization,[21–24] relay synchronization,[25–29] and anti-phase synchronization.[29] Besides the local dynamics of individual nodes that compose complex multilayer networks, synchronization effects depend significantly on the types of connectivity both within a layer and between coupled layers. Relay synchronization was studied in multiplex networks with complex topologies such as scale-free or Erdös–Renyi[25] and random inhomogeneities of a small-world type.[27] Inter-layer synchronization was explored under subsequent de-multiplexing of the structure when the links between nodes and their corresponding replicas were removed randomly or regularly.[14,30] Partial synchronization was studied in population networks with different kinds of fractal and hierarchical connectivity.[32,64–66] The impact of time-varying and time-delayed coupling on synchronous behavior was analyzed in Refs. 26, 31, 32, and 67. Special attention was paid to synchronization in the presence of adaptive coupling.[23,33,68] In Ref. 34, it was shown that inter-layer synchronization can be successfully controlled by noise-modulated coupling between the interacting layers (multiplexing noise).

Nevertheless, most of this research was addressed to attractively coupled dynamical elements and networks, and much less attention was paid to networks of repulsive elements,[35,36,69] or mixed networks,[43–46,70] consisting of both attractive and repulsive elements. However, studying networks with repulsive connectivity undoubtedly deserves more attention and detailed analysis since, for example, it is known that biological networks combine different types of connections to improve synchronization and transmission performance.[71–73] Several studies have shown that the repulsive coupling can play antagonistic roles in the network dynamics. On the one hand, the repulsive coupling can lead to amplitude death.[37–40] On the other hand, it can induce oscillations in excitable systems,[74] as well as regimes of traveling waves and partial synchronization.[35,40] In Ref. 42, it was shown that a small fraction of phase-repulsive links can enhance synchronization in a complex network of non-identical locally coupled Hodgkin–Huxley neurons. As was demonstrated in Ref. 41, the dynamics of a complex network can change essentially if the network layers are characterized by different intra-layer coupling topologies (either attractive or repulsive). Transitions between different synchronous states were analyzed in a network of phase oscillators with attractive and repulsive interactions.[46] Recently, the peculiarities of inter-layer synchronization were uncovered in a two-layer lattice network of attractively and repulsively coupled van der Pol oscillators with attractive inter-layer coupling.[75] It was also indicated that introducing repulsive intra-layer coupling leads to the formation of a complex spatiotemporal structure, which is connected with the appearance of anti-phase oscillations of adjacent nodes in the layers. However, the impact of purely repulsive inter-layer coupling on synchronization of complex multiplex networks has not been studied yet.

Here, we fill this gap and perform a detailed numerical study of synchronization in a bilayer network of repulsively and bidirectionally coupled 2D lattices of van der Pol oscillators. We consider two configurations of the local intra-layer coupling in the interacting lattices: (i) different topologies (repulsive–attractive) and (ii) identical topologies (either attractive–attractive or repulsive–repulsive). The isolated network of repulsively coupled van der Pol oscillators exhibits a labyrinth-like spatiotemporal pattern that was found and described for the first time in Ref. 47. The uncoupled lattice of van der Pol oscillators with an attractive interaction typically shows a regular spiral wave structure. We reveal for the first time that in all the considered cases, the repulsive inter-layer coupling induces *anti-phase* synchronization of complex structures. This phenomenon is diagnosed by using the correlation coefficient between the corresponding pairs of nodes, which is always close or equal to -1 for the anti-phase synchronization regime. We also analyze the competition between the labyrinth-like and the spiral wave pattern when the intra- and inter-layer coupling strengths are varied.

II. NETWORK EQUATIONS

In our numerical simulation, we consider a multiplex of two layers each consisting of $N \times N$ nodes with $N = 50$. The model under study is schematically drawn in Fig. 1. The interacting layers are pairwise and bidirectionally coupled with each other; i.e., there is a one-to-one correspondence between the nodes. Each layer represents a 2D lattice of locally coupled van der Pol oscillators. The dynamics of the bilayer network is described by the following set of equations:

$$\begin{aligned} \dot{x}^l_{i,j} &= y^l_{i,j}, \\ \dot{y}^l_{i,j} &= \varepsilon(1-(x^l_{i,j})^2)y^l_{i,j} - \omega^2 x^l_{i,j} + J_l \frac{\sigma_l}{Q_l} \sum_{m_l,n_l} \left(y^l_{m_l,n_l} - y^l_{i,j}\right) \\ &\quad -\gamma \sum_{k=1}^{2} \left(y^k_{i,j} - y^l_{i,j}\right), \end{aligned} \tag{1}$$

where $x^l_{i,j}, y^l_{i,j}$ are dynamical variables and l labels the layer, $l = 1, 2$. Double subscripts (i, j), where $i, j = 1, \ldots, N = 50$, denote the position on the two-dimensional lattice. The local dynamics of the individual oscillator is controlled by the parameter ε, which denotes the nonlinearity level, and ω is the natural frequency of linear oscillations. We fix these parameters to the values $\varepsilon = 2.0$ and $\omega = 2.0$, which ensure that the local dynamics of each node corresponds to relaxation oscillations.

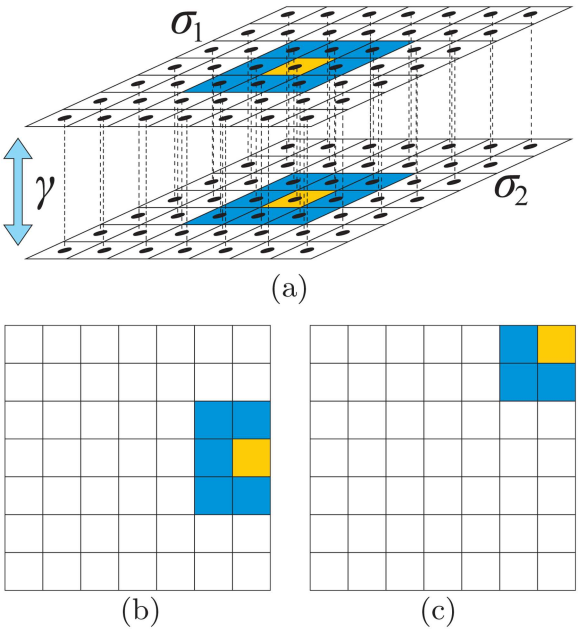

FIG. 1. (a) Schematic representation of a bilayer multiplex network of coupled 2D lattices with a local intra-layer connection. Labels σ_1 and σ_2 denote the intra-layer coupling strengths in the first and second layer, respectively, and γ is the inter-layer coupling strength. (b) and (c) Schemes of the intra-layer coupling topology in an isolated 2D lattice at the edges and corners in the case of no-flux boundary conditions (2). Oscillators coupled with a selected yellow (i,j)th node are colored in blue, and the remaining uncoupled nodes are shown in white.

The intra-layer coupling for each lattice is described by the third term in the second equation of the network (1) and is determined by the intra-layer coupling strength σ_l (k, $l = 1, 2$). The intra-layer coupling topology is defined by the parameter J_l ($l = 1, 2$), which is set to -1 for the repulsive intra-layer coupling and $+1$ for the attractive one.

In our simulation, the bidirectional coupling between the two lattices is considered to be repulsive and is given by the fourth term in the second equation of each lattice (1). The coefficient γ denotes the inter-layer coupling strength.

The quantity Q_l in (1) counts all intra-layer links in both directions for each node of the lth layer and thus represents a combination of all the links with the indices m_l and n_l, which satisfy the following relations:

$$\begin{cases} \max(1, i-1) \leqslant m_l \leqslant \min(N, i+1), \\ \max(1, j-1) \leqslant n_l \leqslant \min(N, j+1). \end{cases} \tag{2}$$

Expressions (2) correspond to no-flux boundary conditions, which are schematically pictured in Figs. 1(b) and 1(c) for an isolated lattice with a local interaction and for different locations of a selected oscillator in the middle of the right edge [Fig. 1(b)] and in the right upper corner [Fig. 1(c)].

The initial conditions for all the dynamical variables of the network (1) are chosen to be random and uniformly distributed within the interval $[-1, 1]$.

The network equation (1) is integrated using the Runge–Kutta 4th order method with the time step $dt = 0.005$. The transient time is chosen to be $T_{\text{tr}} = 10\,000$ time units for all cases under study.

III. DYNAMICAL REGIMES IN UNCOUPLED LAYERS

We start with exploring the dynamics of isolated 2D lattices when there is no coupling between them, i.e., $\gamma = 0$ in (1).

The first lattice in (1) is characterized by the local repulsive intra-layer coupling between the nodes [$J_1 = -1$ in the network (1)]. This type of coupling can be realized, for instance, by an electronic circuit of elements interacting with linear negative differential resistance. Our studies show that due to the repulsive intra-layer coupling, various spatiotemporal patterns can be induced in the lattice, and spiral waves cannot occur there for any initial conditions. Figures 2(a)–2(c) exemplify a typical regime that can be observed in the first isolated lattice of repulsively and locally coupled van der Pol oscillators.

This spatiotemporal structure presents an alternation of "strips," each characterized by in-phase oscillations. However, the oscillation phases of the nodes in adjacent strips are shifted by half a period. This means that the oscillations are anti-phase, and this is clearly seen from the time series plotted in Fig. 2(c) for two different oscillators belonging to adjacent strips. The strips that form the spatiotemporal pattern in the first isolated layer [Fig. 2(a)] have a different length and can be oriented both vertically and horizontally. Similar spatiotemporal patterns have been discovered in a lattice of strongly coupled van der Pol oscillators and described in Ref. 29. These patterns have been called "labyrinth-like structures." At the same time, despite a qualitative similarity between the labyrinth-like patterns in these two lattices, there are significant differences between them. In Ref. 29, such a structure is formed due to the emergence of two coexisting chaotic attractors in the phase space of individual oscillators, which are induced by strong coupling. In contrast, no bistability arises in the lattice under study, and the oscillations of the nodes in neighboring strips differ only by the instantaneous phases [Fig. 2(a)]. The spatiotemporal dynamics of the first isolated lattice of the network (1) is also illustrated by the space-time plot for the $j = 36$th cross section shown in Fig. 2(b). In the case of nonlocal coupling, the structures become regular for long coupling ranges and represent an alternation of strips or squares of oscillators with certain values of the instantaneous phases of oscillations.[75] Nevertheless, the quantitative features of the dynamical regimes that arise for both short and long intra-layer coupling ranges remain very similar. This enables us to assume that the same structure with different spatial topologies can be observed within a wide interval of intra-layer coupling range values.

We now turn to consider dynamical regimes, which can be observed in the second isolated lattice with attractive intra-layer coupling [$J_l = +1$, $l = 2$, in (1)]. This topology corresponds to the case when nodes in an electronic circuit interact through an Ohmic resistance. Our numerical simulations show that only three types of spatiotemporal patterns are typical for the second lattice dynamics when the intra-layer coupling parameter σ_2 is varied. The first type of the spatiotemporal dynamics occurs for very weak intra-layer

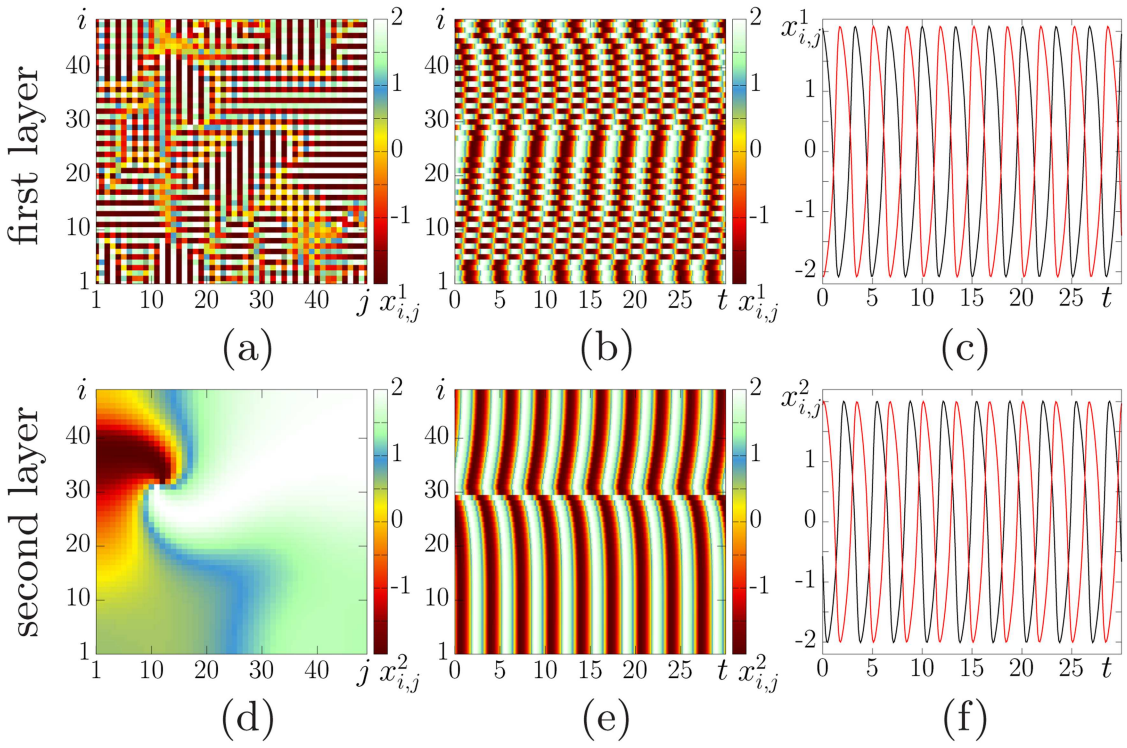

FIG. 2. (a)–(c) Labyrinth-like structure in the first isolated lattice with repulsive intra-layer coupling ($J_1 = -1$) and (d)–(f) a spiral wave in the second isolated layer with attractive intra-layer coupling ($J_2 = 1$). Snapshots of the instantaneous states for the x^1 (a) and x^2 (d) variables; space-time plots of the cross sections for the first layer at $j = 31$ (b) and for the second layer at $j = 12$ (e); time series for two selected elements ($i = 31$, $j = 35$) (red curve) and ($i = 31$, $j = 36$) (black curve) of the first lattice (c) and for ($i = 31$, $j = 12$) (red curve) and ($i = 21$, $j = 12$) (black curve) elements of the second lattice (f). Other parameters: $\sigma_1 = \sigma_2 = 0.1$, $\varepsilon = 2$, $\omega = 2$, and $N = 50$, $\gamma = 0$.

coupling strength σ_2. In this case, the oscillators behave incoherently with respect to each other, and thus, spatially incoherent dynamics is observed in the second lattice.

Increasing σ_2 leads to the formation of spiral wave structures. A different number of spiral waves can coexist in the second lattice for various sets of initial conditions. Spiral waves are observed only for local and short nonlocal intra-layer coupling. It should be noted that for a local interaction, the wave structure is formed within a significantly wider range of the intra-layer coupling strength σ_2 than in the case of nonlocal coupling.

The third spatiotemporal regime distinguished in the second lattice is partial or complete synchronization. It takes place when the oscillators are locally coupled and the intra-layer coupling is essentially strong or when the intra-layer coupling is nonlocal. Note that in this case, spiral waves disappear.

In our calculations, we choose the case when a single spiral wave is observed in the second lattice. As an example, spatiotemporal characteristics of such a structure are depicted in Figs. 2(d)–2(f). As can be seen from the space-time plot for the $j = 12$ cross section passing through the wave center [Fig. 2(e)], the wave front rotates around the wave center. Note that this spiral wave cannot be transformed into a spiral wave chimera since the wave is destroyed when the intra-layer coupling becomes nonlocal. The time series plotted in Fig. 2(f) show that the lattice nodes located in the wave center and outside it demonstrate almost anti-phase oscillations.

It should be noted that all the structures under study presented in Fig. 2 are sufficiently robust and do not change qualitatively and quantitatively when the intra-layer coupling strengths are varied within the interval $\sigma_{1,2} \in [0.05, 0.20]$. These structures are chosen to be the initial states in the first and second lattice. Besides, using these initial states, we have obtained a set of initial conditions for each value of the intra-layer coupling strength $\sigma_{1,2} \in [0.05, 0.20]$ and use them in studying synchronization effects in the multiplex network (1).

IV. SYNCHRONIZATION MEASURE

As a quantitative measure of synchronization between the interacting layers of the network (1), we use the correlation coefficient[21,76] between the corresponding (i, j)th pairs of oscillators of the first and second layer. This quantity is defined as follows:

$$R_{i,j} = \frac{\overline{\tilde{x}^1_{i,j} \cdot \tilde{x}^2_{i,j}}}{\sqrt{\overline{(\tilde{x}^1_{i,j})^2} \cdot \overline{(\tilde{x}^k_{i,j})^2}}}, \quad \tilde{x}^{12}_{i,j} = x^{12}_{i,j} - \overline{x^{12}_{i,j}}, \tag{3}$$

where $\overline{\cdots}$ means time-averaging over $T_{\text{av}} = 10\,000$ time units.

The correlation measure (3) used for arbitrary oscillation modes can attain both positive and negative values. In our numerical studies, we deal with anti-phase synchronization for which $R_{i,j} = -1$ for all (i,j)th pairs of oscillators. Taking into account that the bilayer network under study (1) is heterogeneous (the layers can differ in their intra-layer coupling topology), only approximate effective synchronization is found. Effective anti-phase synchronization is assumed to occur if $R_{i,j} < -0.95$ for all (i,j)th pairs of the network nodes $(i,j = 1,\ldots,N)$. If $R_{i,j} = -1$ for all the network oscillators, then anti-phase synchronization is complete.

V. ANTI-PHASE SYNCHRONIZATION IN MULTIPLEX NETWORKS WITH REPULSIVE INTER-LAYER COUPLING

A. Bilayer network of repulsively and attractively coupled van der Pol oscillators

We first consider the case when the interacting layers of the network (1) differ in the intra-layer coupling topology, i.e., the first layer consists of repulsively coupled van der Pol oscillators, while the second layer represents a 2D lattice of attractively coupled van der Pol oscillators. The spatiotemporal structures depicted in Figs. 2(a) and 2(d) are chosen as initial conditions for the layers.

Our numerical simulations indicate that introducing repulsive inter-layer coupling between the layers in Eq. (1) gives rise to *anti-phase synchronization* in a wide range of the inter-layer coupling strength γ. In this case, the correlation measure (3) becomes negative for all the oscillator pairs of the interacting lattices. It should be noted that in the majority of cases, networks with attractive inter-layer coupling demonstrate in-phase synchronization. At the same time, anti-phase synchronization is a well-known phenomenon that was discovered by Huygens in 1665 for pendulum clocks. Moreover, it was established that this type of synchronization is more stable than in-phase synchronization.[2] Anti-phase synchronization in a multilayer network with attractive inter-layer coupling has been described in Ref. 29, where anti-phase relay synchronization has been revealed and explored in a heterogeneous triplex network of coupled 2D lattices. To describe and illustrate anti-phase synchronization in detail, we fix the intra-layer coupling strengths $\sigma_1 = 0.1$ and vary the second one within the range $\sigma_2 \in [0.05, 0.15]$ with a sample step $\Delta\sigma_2 = 0.01$ or fix $\sigma_2 = 0.1$ and vary $\sigma_1 \in [0.05, 0.15]$ with a step $\Delta\sigma_1 = 0.01$. The repulsive inter-layer coupling strength γ increases from 0 to 1 with a step size $\Delta\gamma = 0.01$.

To have a full overview of the network (1) dynamics, we plot two 2D diagrams of synchronous and desynchronized regimes in the (σ_2, γ) parameter plane [for the fixed $\sigma_1 = 0.1$, Fig. 3(a)] and in the (σ_1, γ) parameter plane [for the fixed $\sigma_2 = 0.1$, Fig. 3(b)] by using the values of $\langle R \rangle$, where the angular brackets mean that the values of the correlation coefficient (3) are globally averaged over all the oscillator pairs (i,j). We count the number of synchronized (in the sense of anti-phase synchronization condition $R_{i,j} \le -0.95$) oscillator pairs N_s and then normalize it to the whole number of nodes in each lattice N^2. The color scheme in the diagrams (Fig. 3) corresponds to the ratio N_s/N^2.

In order to get better insight into synchronization effects in the network (1), three different regions are distinguished in the 2D diagrams in Fig. 3, namely, desynchronization region DS, where the spatiotemporal behavior in both lattices is different ($N_s/N^2 < 1$), and two regions of anti-phase synchronization S_{LS} and S_{SW} for which $N_s/N^2 = 1$. Within region S_{LS}, a spatiotemporal structure, which is similar to the initial state in the first lattice [Fig. 2(a)], is observed in both layers, while anti-phase synchronization of the initial spiral wave [Fig. 2(d)] occurs inside region S_{SW}. The boundaries between the indicated regimes are denoted by dotted curves. It is clearly seen from Fig. 3 that inter-layer synchronization has a strong and sufficiently complicated dependence on the relationship between σ_1 and σ_2. When the values of both intra-layer coupling strengths are close to each other, inter-layer synchronization takes place for a substantially stronger inter-layer coupling. As follows from Fig. 3(a), when σ_2 exceeds $\sigma_1 = 0.1$, the threshold level for synchronization in the parameter γ decreases noticeably. In contrast, the diagram in Fig. 3(b) shows that when $\sigma_1 \gg \sigma_2 = 0.1$, the lattices either become synchronized only at very large values of γ or remain desynchronized.

The dependence of the globally averaged correlation measure $\langle R \rangle$ on the inter-layer coupling strength γ plotted in Fig. 3(c) for several values of the intra-layer coupling strength σ_2 and for fixed $\sigma_1 = 0.1$ shows that effective anti-phase synchronization is observed when $\sigma_2 < \sigma_1$. In this case, starting with $\gamma \approx 0.4$, $\langle R \rangle$ becomes less than -0.95 but never reaches -1. As is seen from the diagram in Fig. 3(a), this type of synchronization is related to synchronous labyrinth-like patterns (region S_{LS}). The quantity $\langle R \rangle$ is almost exactly equal to -1, which corresponds to complete anti-phase synchronization, can be achieved only for $\sigma_2 > \sigma_1$ when we enter region S_{SW} inside which spiral wave structures are synchronized [Fig. 3(a)]. The same peculiarity of synchronization is observed when $\sigma_2 = 0.1$ is fixed and σ_1 is varied [Fig. 3(d)]. However, in this case, complete anti-phase synchronization of spiral waves takes place when $\sigma_1 < \sigma_2$. Besides, as follows from the plot $\langle R \rangle(\gamma)$ [Fig. 3(d)], as σ_2 becomes larger than σ_1, effective synchronization of labyrinth-like patterns is gradually destroyed even for significantly strong inter-layer coupling γ.

Inside region DS in the 2D diagrams (Fig. 3), the spiral wave in the second layer is destroyed even for small values of γ, and the labyrinth-like structure observed in the first lattice [Fig. 4(a)] induces a new but very similar state in the second layer, which is shown in Fig. 4(d). However, due to a weak inter-layer coupling strength ($\gamma \le 0.3$), these two spatiotemporal structures are not synchronized, which follows from the spatial distribution of the local correlation coefficient $R_{i,j}$ values plotted in Fig. 4(g). It is interesting to note that the repulsive inter-layer interaction in the network always leads to the anti-phase oscillatory regime. For this reason, the synchronization measure $R_{i,j}$ always attains negative values. This phenomenon is observed for almost the whole ranges of γ and $\sigma_{1,2}$ under study. The anti-phase dynamics of the network (1) is well visible from the comparison of the snapshots for the first and second layer, which are illustrated in Figs. 4(a) and 4(d), respectively. At the same time, in region DS, only a minor part of the oscillator pairs is synchronized ($R_{i,j} \approx -1$), while the main part of the network nodes is characterized by the values of $R_{i,j} > -1$ [Fig. 4(g)]. This circumstance can be explained by the fact that the instantaneous phases of the symmetric oscillators are shifted relative to each other by less than half a period.

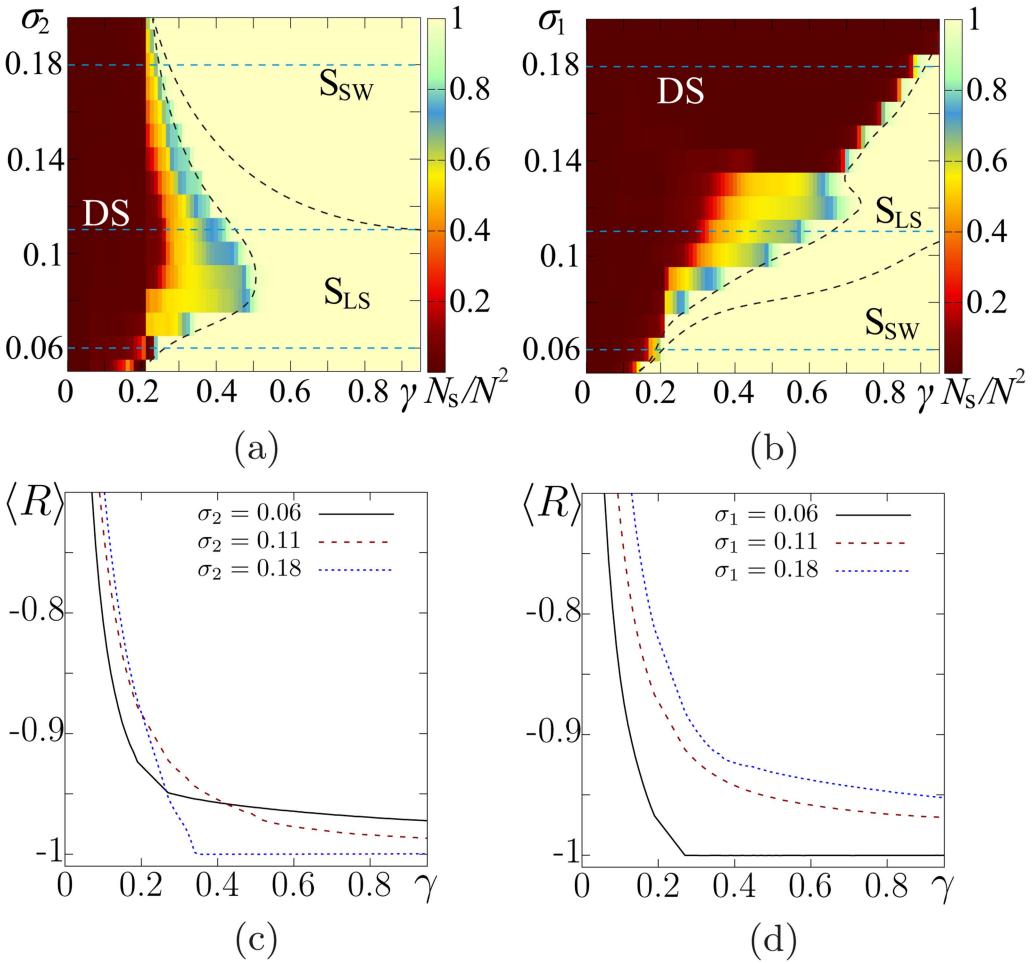

FIG. 3. 2D diagrams of synchronous and desynchronized regimes in the network (1) in the (σ_2, γ) parameter plane at $\sigma_1 = 0.1$ (a) and in the (σ_1, γ) parameter plane at $\sigma_2 = 0.1$ (b). The color scale corresponds to the ratio of synchronized nodes N_s to the whole number of oscillator pairs N^2. DS denotes the desynchronization region, and S_{LS} and S_{SW} are synchronization regions of the initial labyrinth-like structure [Fig. 2(a)] and the original spiral wave [Fig. 2(d)], respectively. The dotted curves indicate the boundaries between the regions. Dependences of the globally averaged correlation coefficient $\langle R \rangle$ on γ for several values of σ_2 at $\sigma_1 = 0.1$ (c) and of σ_1 at $\sigma_2 = 0.1$ (d). The sections in (c) and (d) correspond to the blue dashed horizontal lines in (a) and (b). Parameters: $J_1 = -1$, $J_2 = 1$, $\varepsilon = 2$, $\omega = 2$, and $N = 50$.

As the repulsive inter-layer coupling strength γ grows, anti-phase synchronization occurs in the network (1) and is observed inside regions S_{LS} and S_{SW} shaded light yellow in the 2D diagrams (Fig. 3). Within region S_{LS}, the spatiotemporal structures in the lattices represent the combination of both initial regimes (Fig. 2). The patterns observed in the first and second lattice for $\gamma = 0.45$ are depicted in Figs. 4(b) and 4(e), respectively. These states now combine the features of both the labyrinth-like structure and the spiral wave. They are characterized by a complex spatial shape of the labyrinth-like pattern and the presence of a spiral wave center. As can be seen from the spatial distribution of the correlation measure $R_{i,j}$ shown in Fig. 4(h), all the values of $R_{i,j}$ are very close to each other but are not strictly equal to -1. Therefore, we cannot conclude complete anti-phase synchronization.

Significant changes in the network dynamics take place when we pass from region S_{LS} to region S_{SW} in the diagrams in Fig. 3. The labyrinth-like structure in the first lattice is fully destroyed and replaced with a spiral wave, which is induced by the second layer. Snapshots of the resulting wave structures in the first and second layer are presented in Figs. 4(c) and 4(f), respectively. It is clearly seen that these waves are in anti-phase relative to each other. Moreover, complete anti-phase synchronization is realized within region S_{SW}. This fact is confirmed by the spatial distribution of $R_{i,j}$, which is plotted in Fig. 4(i). All the (i,j)th oscillator pairs, except a very small region around the wave center, are characterized by the correlation measure $R_{i,j} = -1$. It was earlier shown that oscillators belonging to spiral wave centers cannot be completely synchronized.[77,78]

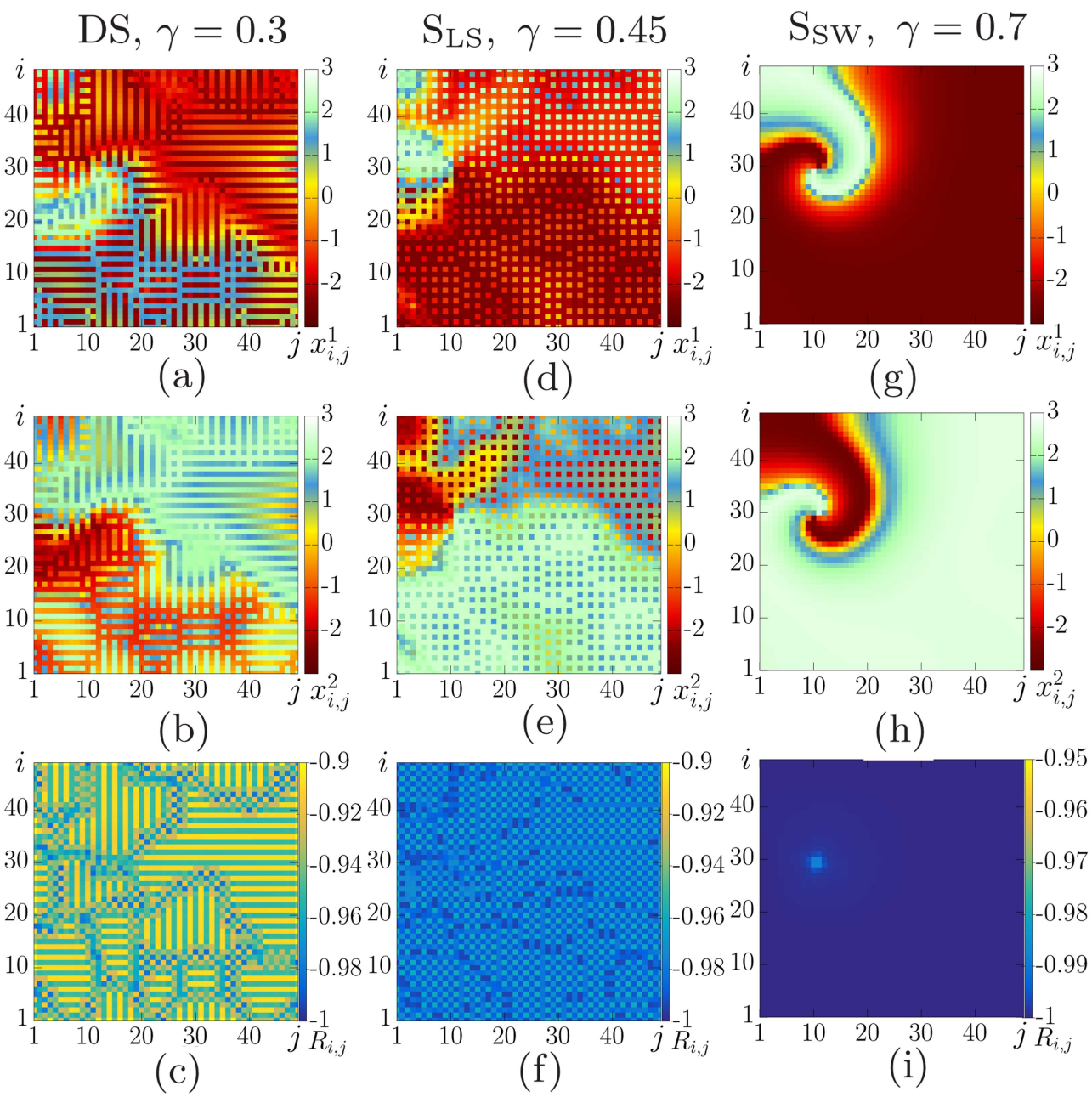

FIG. 4. Typical spatiotemporal structures observed in three regions of the 2D diagrams (Fig. 3) at (a), (d), and (g) $\gamma = 0.3$ (region DS), (b), (e), and (h) $\gamma = 0.45$ (region S_{LS}), and (c), (f), and (i) $\gamma = 0.7$ (region S_{SW}). Snapshots of the instantaneous states for the x^1 (upper row) and x^2 (middle row) variables and spatial distributions of local correlation measure R_{ij} (lower row). Other parameters: $J_1 = -1$, $J_2 = 1$, $\sigma_1 = 0.1$, $\sigma_2 = 0.13$, $\varepsilon = 2$, $\omega = 2$, and $N = 50$.

Thus, when studying the dynamics of the repulsively coupled 2D lattices (1), two important facts can be highlighted: (i) anti-phase synchronization takes place in the bilayer network and (ii) the spiral wave regime in the second layer with attractive intra-layer coupling is less stable than the labyrinth-like structure in the first layer with repulsive intra-layer coupling. The spiral wave can suppress the structure in the first lattice only when the intra-layer coupling strength σ_2 is larger than σ_1. In other cases, the

labyrinth-like structure suppresses the spiral wave or both lattices exhibit spatiotemporal regimes, which combine the peculiarities of both structures.

B. Transformation of synchronized spatiotemporal structures on the transition between dynamical regimes

We now consider in detail how the synchronous spatiotemporal structures can change, while one moves from region S_{LS} to S_{SW} in the diagram in Fig. 3(a). To illustrate this process, we fix the repulsive inter-layer coupling strength as $\gamma = 0.6$ and the repulsive intra-layer coupling strength in the first layer as $\sigma_1 = 0.1$ and increase the attractive intra-layer coupling strength in the second layer σ_2.

When $\sigma_2 = 0.1$, identical synchronous labyrinth-like structures (which are anti-phase with respect to each other) are observed in both lattices. A typical snapshot of such a state is exemplified in Fig. 5(a). It is seen that the spatiotemporal structure looks like a labyrinth-like pattern but also includes certain peculiarities of a spiral wave. The corresponding spatial distribution of correlation measure $R_{i,j}$ is given in Fig. 5(d) and indicates that most of the $R_{i,j}$ values belong to the interval $[-1; -0.95]$. According to the synchronization criteria, this gives evidence that effective anti-phase synchronization takes place.

The observed spatiotemporal structure begins to change significantly when the coupling strength σ_2 increases and approaches the boundary between regions S_{LS} and S_{SW} shown in Fig. 3(a). The snapshot of the modified pattern pictured in Fig. 5(b) corresponds to the case when σ_2 is very close to this boundary [when one moves from left to right in the diagram in Fig. 3(a)]. This structure is now characterized by the coexistence of two types of patterns, namely, a "strip" with similar instantaneous phases and a "strip" in which adjacent oscillators are generally in anti-phase to each other. At the same time, the spatiotemporal structures in the interacting layers are noticeably more synchronous than in the previous case. As can be seen from the spatial distribution of $R_{i,j}$ presented in Fig. 5(e), in this case, $R_{i,j} \in [-1; -0.97]$.

Inside region S_{SW} in the diagram in Fig. 3(a), both layers are synchronized in a spiral wave mode, which is illustrated by the snapshot shown in Fig. 5(c) for $\sigma_2 = 0.14$. The synchronous structure corresponds to a single spiral wave without any footprints from a labyrinth-like structure. Moreover, the spatial distribution of $R_{i,j}$ plotted in Fig. 5(f) indicates that complete anti-phase synchronization takes place in the network (1) since $R_{i,j} = -1$ for all network nodes except a small region around the wave center.

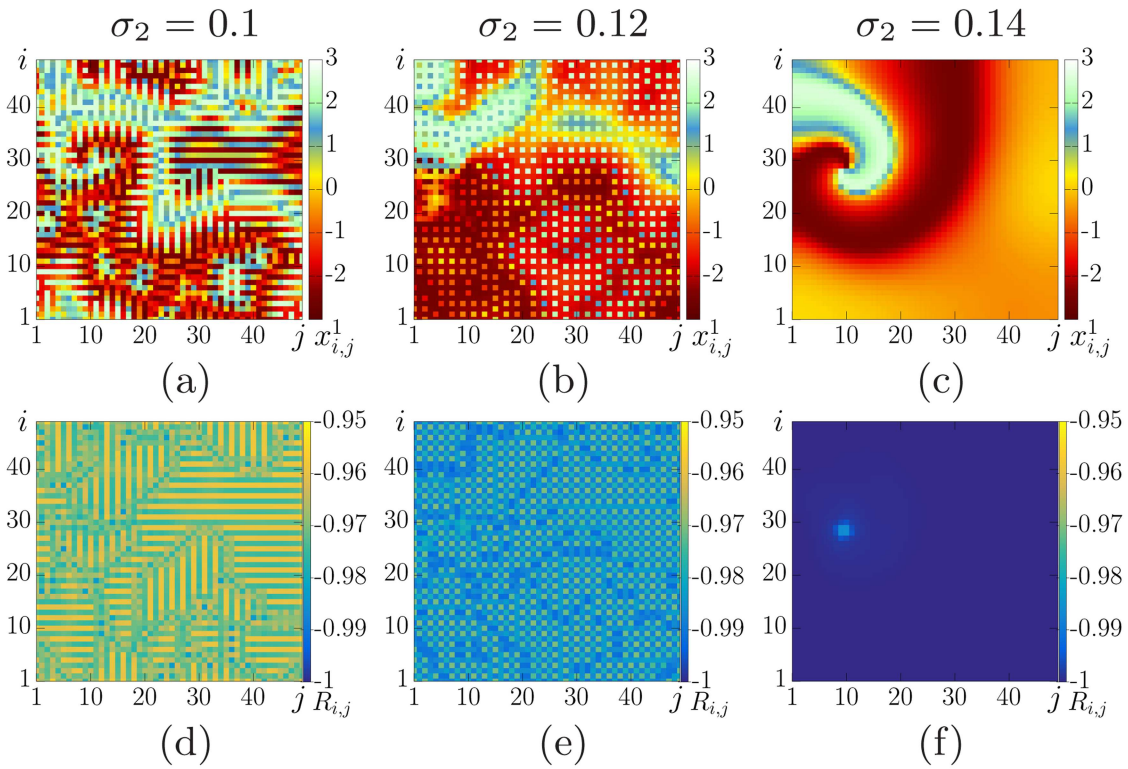

FIG. 5. Changes in synchronous spatiotemporal patterns when one moves from region S_{LS} to S_{SW} in the 2D diagram [Fig. 3(a)]. Snapshots of the instantaneous values of the x^1 variable (upper row) and spatial distributions of $R_{i,j}$ (lower row) for (a) and (d) $\sigma_2 = 0.1$, (b) and (e) $\sigma_2 = 0.12$, and (c) and (f) $\sigma_2 = 0.14$. Other parameters: $J_1 = -1$, $J_2 = 1$, $\sigma_1 = 0.1$, $\gamma = 0.6$, $\varepsilon = 2$, $\omega = 2$, and $N = 50$.

Our calculations have demonstrated that similar modifications take place for the synchronous structures in the case when σ_2 is fixed and σ_1 is varied within the range shown in the diagram in Fig. 3(b). However, these transformations happen in the reverse order as compared with those described above.

C. Bilayer network with identical topology of the intra-layer coupling

We now address the case of bidirectionally and repulsively coupled 2D lattices of van der Pol oscillators (1) when the layers are characterized by the same topology of the intra-layer coupling. At first, let the intra-layer couplings be attractive, i.e., $J_l = +1$ $(l = 1, 2)$ in Eq. (1) for both layers. In this case, similar spiral waves as shown in Fig. 2(d) are observed in the uncoupled lattices. Our calculations demonstrate that the layers begin to synchronize even for very weak repulsive inter-layer coupling γ when both intra-layer coupling strengths $\sigma_{1,2}$ are varied within the range [0.05, 0.2]. However, we can note that the initial structures can become unstable for certain values of γ and $\sigma_{1,2}$ and transform to spiral waves with different spatial topologies. The latter may correspond to either a different location of wave centers or to a different number of coexisting spiral waves. At the same time, our studies show that inter-layer synchronization of wave patterns is complete and anti-phase for all the cases. This fact is confirmed by the results for the correlation measure $R_{i,j}$ (3), which is strictly equal to -1 for all the network nodes except for the wave center oscillators.

The synchronization effects appear to be more interesting when the intra-layer coupling in both lattices is repulsive, i.e., $J_l = -1$, $l = 1, 2$, in (1). The layers exhibit very similar labyrinth-like structures as illustrated in Fig. 2(d) when there is no inter-layer coupling between them. Moreover, these patterns are observed when the intra-layer coupling strengths $\sigma_{1,2}$ are varied within the interval [0.05, 0.2]. A 2D diagram of synchronous and asynchronous regimes in the network (1) is plotted in the (σ_2, γ) parameter plane for fixed $\sigma_1 = 0.1$ and presented in Fig. 6(a). As before, three different regions are distinguished in the diagram and correspond to desynchronized behavior (region DS) and complete and effective inter-layer synchronization (regions CS and ES, respectively). As in the previous case, inter-layer synchronization is also characterized by a sufficiently low threshold level in the inter-layer coupling γ for the whole range of σ_2 variation. The threshold value is minimal (about zero) in the vicinity of $\sigma_1 = \sigma_2 = 0.1$ and then monotonically increases when the difference between the intra-layer coupling strengths grows.

As can be seen from the diagram [Fig. 6(a)], the synchronization region (shaded light yellow) is divided by the dotted lines into two different subregions with the CS and ES notations. Increasing σ_2 leads to a change in the synchronization type. When σ_2 is sufficiently small, complete anti-phase synchronization of labyrinth-like structures [region CS in Fig. 6(a)] takes place in the network. This fact is confirmed by the dependences $\langle R\rangle$ on γ calculated for several values of σ_2 at the fixed $\sigma_1 = 0.1$ and plotted in Fig. 6(b). It is seen that complete synchronization ($\langle R\rangle = -1$) is achieved in the network starting already with an extremely weak inter-layer coupling strength γ when $\sigma_2 < \sigma_1$. The spatial distribution of $R_{i,j}$ shown in Fig. 6(c) is homogeneous and corresponds exactly to $R_{i,j} = -1$

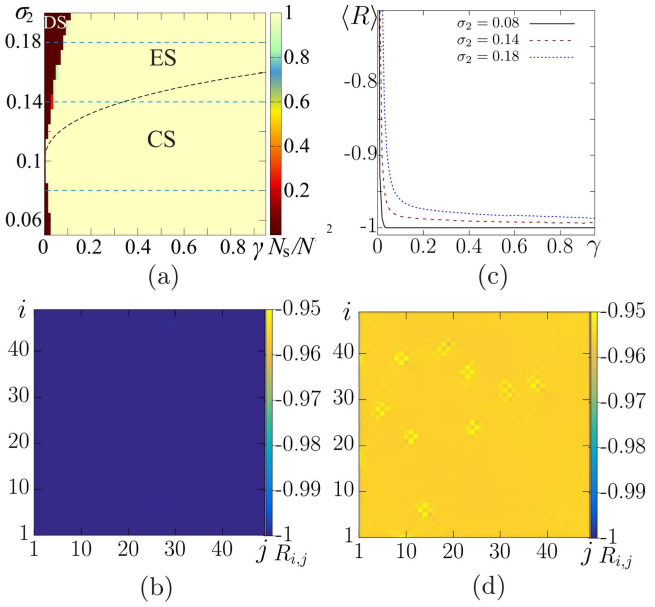

FIG. 6. (a) 2D diagram of synchronous and desynchronized regimes in the network (1) in the (σ_2, γ) parameter plane when both layers have repulsive intra-layer coupling. The color scale corresponds to the ratio of synchronized nodes N_s to the whole number of oscillator pairs N^2. DS denotes the desynchronization region, and CS and ES regions correspond to complete synchronization and effective synchronization, respectively. The dotted curve indicates the boundary between the synchronization regions. (b) Dependences of the globally averaged correlation coefficient $\langle R\rangle$ on γ for several values of σ_2. (c) and (d) Spatial distributions of local correlation measure $R_{i,j}$ values for $\gamma = 0.2$ and (c) $\sigma_2 = 0.07$ (region CS) and (d) $\sigma_2 = 0.17$ (region ES). The sections in (b) correspond to the blue dashed horizontal lines in (a). Other parameters: $J_1 = J_2 = -1$, $\sigma_1 = 0.1$, $\varepsilon = 2$, $\omega = 2$, and $N = 50$.

for all the network nodes. It it worth noting that the complete synchronization (CS) region expands in the intra-layer coupling strength σ_2 (up to $\sigma_2 = 0.15$ at $\gamma = 1$) when the repulsive inter-layer coupling becomes stronger [Fig. 6(a)]. When $\sigma_2 > \sigma_1$, complete synchronization is no longer observed and only effective anti-phase synchronization [region ES in the diagram in Fig. 6(a)] takes place between the layers within almost the whole range of inter-layer coupling strength γ variation. As follows from the dependences $\langle R\rangle(\gamma)$ [Fig. 6(b)] and the distribution, the local synchronization measure $R_{i,j}$ [Fig. 6(d)], in this case, $-1 < \langle R\rangle < -0.95$ and $R_{i,j} \approx -0.955$ for all the (i, j)th oscillator pairs, satisfies the imposed synchronization condition.

VI. CONCLUSION

We have studied numerically inter-layer synchronization in a multiplex bilayer network of pairwise and bidirectionally coupled 2D lattices of locally coupled van der Pol oscillators. We have explored two types of the intra-layer interaction. In the first case, the intra-layer connection in the first layer is repulsive and a labyrinth-like structure is typical for the isolated layer. Oscillators of the second layer are coupled attractively and demonstrate a spiral

wave regime. In the second case, the intra-layer coupling in both lattices has the same topology—repulsive or attractive. All the mentioned coupling types have a simple radiophysical interpretation, namely, the interaction through an Ohmic resistance for the attractive connection and via an active element with a negative differential resistance for the repulsive coupling.

It has been shown for the first time that mutual synchronization of the two repulsively coupled layers can be achieved even when the interacting lattices differ in their intra-layer coupling. We have also revealed that the repulsive inter-layer interaction between the layers always induces anti-phase synchronization of spatiotemporal patterns. In our research, synchronous behavior is diagnosed by calculating the local correlation coefficient between the symmetrical pairs of the network nodes. This synchronization measure is always close to -1 in the case of effective anti-phase synchronization and is exactly equal to -1 for the complete anti-phase synchronization regime. We have found that due to the repulsive inter-layer coupling, the symmetrical elements of the interacting layers demonstrate anti-phase oscillations with respect to each other.

Our numerical simulations have shown that the synchronization effects and the synchronous structures in the lattices significantly depend on the relationship between the intra-layer coupling strengths σ_1/σ_2. In particular, the synchronization threshold of the inter-layer coupling strength noticeably changes when this ratio is varied. If the coupling strength σ_2 is either less or equal to σ_1, then complete synchronization takes place. If $\sigma_1 \gg \sigma_2$, the synchronization can only be partially effective.

It has been established that the spiral wave pattern in the second lattice is fully destroyed already for a sufficiently weak inter-layer coupling, and the labyrinth-like structure is observed in this layer. When the inter-layer interaction becomes stronger, the spatiotemporal regimes in the layers represent a combination of both initial regimes. However, when $\sigma_2 \gg \sigma_1$, a single spiral wave is observed in both lattices starting from a certain threshold value of γ. The latter significantly decreases as the ratio σ_2/σ_1 grows. Moreover, in this case, the network under study demonstrates the most synchronous oscillations.

Thus, the bidirectional repulsive inter-layer coupling induces anti-phase synchronization in the network and the emergence of structures, which cannot be obtained in the isolated lattices, i.e., the spiral wave in the layer with repulsive elements and the labyrinth-like structure in the lattice with attractive nodes. It should be noted that the transition between the two synchronous regimes is noticeably different from the scenario, which occurs in the attractively coupled two-layer network.[75] In the present case, the transition is accompanied by the structural changes in the labyrinth-like pattern. The lengths of "strips" with similar phases become significantly shorter up to the case when most "strips" transform to "dots." When one crosses the boundary between the regimes, the labyrinth-like structure fully disappears and anti-phase synchronized spiral waves are observed in both layers.

In the framework of the present research, we have dealt with 2D lattices of locally coupled van der Pol oscillators. As an outlook, in the future, it is planned to explore how the nonlocal intra-layer coupling can affect the synchronization effects and the competitive behavior between labyrinth-like and spiral wave patterns.

DEDICATION

We dedicate this paper to the memory of Vadim S. Anishchenko, who was our inspiring teacher, mentor, colleague, and friend.

ACKNOWLEDGMENTS

This work was supported by the Deutsche Forschungsgemeinschaft (DFG, German Research Foundation) (Projektnummer 163436311—SFB 910) and by RFBR and DFG according to Research Project No. 20-52-12004.

DATA AVAILABILITY

The data that support the findings of this study are available within the article.

REFERENCES

[1] V. S. Anishchenko, T. E. Vadivasova, and G. I. Strelkova, *Deterministic Nonlinear Systems*, Springer Series in Synergetics (Springer International Publishing, Cham, 2014), ISBN: 978-3-319-06870-1.
[2] A. Pikovsky, M. Rosenblum, and J. Kurths, *Synchronization* (Cambridge University Press, 2001), ISBN: 9780521533522.
[3] V. I. Nekorkin and M. G. Velarde, *Synergetic Phenomena in Active Lattices*, Springer Series in Synergetics (Springer, Berlin, 2002), ISBN: 978-3-642-62725-5.
[4] G. V. Osipov, J. Kurths, and C. Zhou, *Synchronization in Oscillatory Networks*, Springer Series in Synergetics (Springer, Berlin, 2007), ISBN: 978-3-540-71268-8.
[5] A. Balanov, N. Janson, D. Postnov, and O. Sosnovtseva, *Synchronization: From Simple to Complex* (Springer Science & Business Media, 2008).
[6] S. Boccaletti, A. N. Pisarchik, and A. Amann, *Synchronization* (Cambridge University Press, 2018), ISBN 9781107056268.
[7] S. Hong and Y. Chun, Soc. Choice Welf. **34**, 441–454 (2010).
[8] E. Schöll, Nova Acta Leopold. **425**, 67–95 (2020).
[9] S. Boccaletti, G. Bianconi, R. Criado, J. Gómez-Gardeñes, M. Romance, I. Sendiña-Nadal, Z. Wang, and M. Zanin, Phys. Rep. **544**, 1–122 (2014).
[10] M. Kivela, A. Arenas, M. Barthelemy, J. P. Gleeson, Y. Moreno, and M. A. Porter, J. Complex Netw. **2**, 203–271 (2014).
[11] M. L. Pecora, F. Sorrentino, M. A. Hagerstrom, E. T. Murphy, and R. Roy, Nat. Commun. **5**, 4079 (2014).
[12] S. Jalan and A. Singh, Europhys. Lett. **113**, 30002 (2016).
[13] L. V. Gambuzza, M. Frasca, and J. Gómez-Gardeñes, Europhys. Lett. **110**, 20010 (2015).
[14] R. Sevilla-Escoboza, I. Sendiña-Nadal, I. Leyva, R. Gutiérrez, M. J. Buldú, and S. Boccaletti, Chaos **26**, 065304 (2016).
[15] I. Leyva, R. Sevilla-Escoboza, I. Sendiña-Nadal, R. Gutiérrez, J. Buldú, and S. Boccaletti, Sci. Rep. **7**, 45475 (2017).
[16] S. Rakshit, S. Majhi, K. B. Bera, S. Sinha, and D. Ghosh, Phys. Rev. E **96**, 062308 (2017).
[17] I. Leyva, I. Sendiña-Nadal, J. A. Almendral, A. Navas, S. Olmi, and S. Boccaletti, Phys. Rev. E **88**, 042808 (2013).
[18] X. Zhang, S. Boccaletti, S. Guan, and Z. Liu, Phys. Rev. Lett. **114**, 038701 (2015).
[19] S. Jalan, V. Rathore, A. D. Kachhvah, and A. Yadav, Phys. Rev. E **99**, 062305 (2019).
[20] A. D. Kachhvah and S. Jalan, New J. Phys. **21**, 015006 (2019).
[21] A. Bukh, G. Strelkova, and V. Anishchenko, Nelineinaya Din. **14**, 419–433 (2018).
[22] G. I. Strelkova, T. E. Vadivasova, and V. S. Anishchenko, Regul. Chaotic Dyn. **23**, 948–960 (2018).
[23] D. V. Kasatkin and V. I. Nekorkin, Chaos **28**, 093115 (2018).
[24] V. E. Rybalova, E. T. Vadivasova, I. G. Strelkova, S. V. Anishchenko, and S. A. Zakharova, Chaos **29**, 033134 (2019).
[25] I. Leyva, I. Sendiña-Nadal, R. Sevilla-Escoboza, V. Vera-Avila, P. Chholak, and S. Boccaletti, Sci. Rep. **8**, 8629 (2018).

[26]J. Sawicki, I. Omelchenko, A. Zakharova, and E. Schöll, Phys. Rev. E **98**, 062224 (2018).
[27]F. Drauschke, J. Sawicki, R. Berner, I. Omelchenko, and E. Schöll, Chaos **30**, 051104 (2020).
[28]E. Rybalova, G. Strelkova, E. Schöll, and V. Anishchenko, Chaos **30**, 061104 (2020).
[29]I. Shepelev, A. Bukh, G. Strelkova, and V. Anishchenko, Chaos, Solitons Fractals **143**, 110545 (2021).
[30]E. Rybalova, G. Strelkova, and V. Anishchenko, Chaos, Solitons Fractals **142**, 110477 (2021).
[31]D. Kasatkin, S. Yanchuk, E. Schöll, and V. Nekorkin, Phys. Rev. E **96**, 062211 (2017).
[32]J. Sawicki, I. Omelchenko, A. Zakharova, and E. Schöll, Eur. Phys. J. B **92**, 54 (2019).
[33]R. Berner, J. Fialkowski, D. Kasatkin, V. Nekorkin, S. Yanchuk, and E. Schöll, Chaos **29**, 103134 (2019).
[34]T. Vadivasova, A. Slepnev, and A. Zakharova, Chaos **30**, 091101 (2020).
[35]L. Tsimring, F. N. Rulkov, L. M. Larsen, and M. Gabbay, Phys. Rev. Lett. **95**, 014101 (2005).
[36]V. A. Pimenova, S. D. Goldobin, M. Rosenblum, and A. Pikovsky, Sci. Rep. **6**, 38518 (2016).
[37]E. Ullner, A. Zaikin, E. Volkov, and J. Ojalvo, Phys. Rev. Lett. **99**, 148103 (2007).
[38]C. Hens, O. Olusola, P. Pal, and S. Dana, Phys. Rev. E **88**(3), 034902 (2013).
[39]C. Hens, P. Pal, S. Bhowmick, P. Roy, A. Sen, and S. Dana, Phys. Rev. E **89**(3), 032901 (2014).
[40]M. Nandan, C. Hens, P. Pal, and S. Dana, Chaos **24**, 043103 (2014).
[41]S. Jalan, S. Ghosh, and B. Patra, Chaos **27**, 101104 (2017).
[42]I. Leyva, I. Sendina-Nadal, J. Almendral, and M. Sanjuán, Phys. Rev. E **74**, 056112 (2006).
[43]D. Iatsenko, S. Petkoski, P. McClintock, and A. Stefanovska, Phys. Rev. Lett. **110**, 064101 (2013).
[44]V. Vlasov, E. E. Macau, and A. Pikovsky, Chaos **24**, 023120 (2014).
[45]T. Qiu, S. Boccaletti, I. Bonamassa, Y. Zou, J. Zhou, Z. Liu, and S. Guan, Sci. Rep. **6**, 1 (2016).
[46]E. Teichmann and M. Rosenblum, Chaos **29**, 093124 (2019).
[47]I. Shepelev and V. Anishchenko, Commun. Nonlinear Sci. Numer. Simul. **93**, 105513 (2021).
[48]J. P. Menck, J. Heitzig, J. Kurths, and H. Joachim Schellnhuber, Nat. Commun. **5**, 3969 (2014).
[49]B. Wang, H. Suzuki, and K. Aihara, Sci. Rep. **6**, 26596 (2016).
[50]G. Buzsaki, *Rhythms of the Brain* (Oxford University Press, 2006).
[51]L. Ramlow, J. Sawicki, A. Zakharova, J. Hlinka, J. C. Claussen, and E. Schöll, Europhys. Lett. **126**, 50007 (2019).
[52]M. Gerster, R. Berner, J. Sawicki, A. Zakharova, A. Škoch, J. Hlinka, K. Lehnertz, and E. Schöll, Chaos **30**, 123130 (2020).
[53]R. Berner, S. Vock, E. Schöll, and S. Yanchuk, Phys. Rev. Lett. **126**, 028301 (2021).
[54]M. Girvan and M. E. J. Newman, Proc. Natl. Acad. Sci. U.S.A. **99**, 7821–7826 (2002).
[55]H. Aoyama, Y. Fujiwara, Y. Ikeda, and W. Souma, *Macro-Econophysics: New Studies on Economic Networks and Synchronization* (Cambridge University Press, 2017).
[56]L. Danon, A. P. Ford, T. House, C. P. Jewell, M. J. Keeling, G. O. Roberts, J. V. Ross, and M. C. Vernon, Interdiscip. Perspect. Infect. Dis. **2011**, 284909.
[57]M. Salathé and J. H. Jones, PLoS Comput. Biol. **6**, e1000736 (2010).
[58]M. Barahona and M. L. Pecora, Phys. Rev. Lett. **89**, 054101 (2002).
[59]H. S. Strogatz, Nature **410**, 268–276 (2001).
[60]R. Albert and L. A. Barabási, Rev. Mod. Phys. **74**, 47 (2002).
[61]M. K. Lee, B. Min, and I. K. Goh, Eur. Phys. J. B **88**, 48 (2015).
[62]M. De Domenico, C. Granell, A. M. Porter, and A. Arenas, Nat. Phys. **12**, 901–906 (2016).
[63]G. R. Andrzejak, G. Ruzzene, and I. Malvestio, Chaos **27**, 053114 (2017).
[64]J. Hizanidis, E. Panagakou, I. Omelchenko, E. Schöll, P. Hövel, and A. Provata, Phys. Rev. E **92**, 012915 (2015).
[65]T. Chouzouris, I. Omelchenko, A. Zakharova, J. Hlinka, P. Jiruska, and E. Schöll, Chaos **28**, 045112 (2018).
[66]G. Argyropoulos and A. Provata, Front. Appl. Math. Stat. **5**, 35 (2019).
[67]A. Buscarino, M. Frasca, V. L. Gambuzza, and P. Hövel, Phys. Rev. E **91**, 022817 (2015).
[68]R. Berner, J. Sawicki, and E. Schöll, Phys. Rev. Lett. **124**, 088301 (2020).
[69]C. Van Vreeswijk, L. Abbott, and B. G. Ermentrout, J. Comput. Neurosci. **1**, 313–321 (1994).
[70]H. Hong and H. S. Strogatz, Phys. Rev. Lett. **106**, 054102 (2011).
[71]G. Balázsi, A. Cornell-Bell, B. A. Neiman, and F. Moss, Phys. Rev. E **64**, 041912 (2001).
[72]Q. Wang, G. Chen, and M. Perc, PLoS One **6**, e15851 (2011).
[73]I. M. Rabinovich, P. Varona, I. A. Selverston, and D. H. Abarbanel, Rev. Mod. Phys. **78**, 1213 (2006).
[74]T. Yanagita, T. Ichinomiya, and Y. Oyama, Phys. Rev. E **72**, 056218 (2005).
[75]I. Shepelev, S. Muni, and T. Vadivasova, Chaos **31**, 021104 (2021).
[76]V. A. Bukh, E. Schöll, and V. Anishchenko, Chaos **29**, 053105 (2019).
[77]A. Bukh, G. Strelkova, and V. Anishchenko, Chaos, Solitons Fractals **139**, 110002 (2020).
[78]V. A. Bukh and S. V. Anishchenko, Russ. J. Nonlinear Dyn. **16**, 243–257 (2020).